Case Studies in Thermal Engineering 45 (2023) 102907

Contents lists available at ScienceDirect

Case Studies in Thermal Engineering

journal homepage: www.elsevier.com/locate/csite

Darcy number influence on natural convection around porous cylinders in an enclosure using Darcy- Brinkman-Forchheimer model: LBM study

B. Shruti [a], Md. Mahbub Alam [b], A. Parkash [c], S. Dhinakaran [a,*]

[a] The Centre for Fluid Dynamics, Department of Mechanical Engineering, Indian Institute of Technology Indore, Simrol, Indore, 453 552, India
[b] Center for Turbulence Control, Harbin Institute of Technology (Shenzhen), Shenzhen, 518055, China
[c] Department of Mathematics, Indian Institute of Technology Indore, Simrol, Indore, 453 552, India

ARTICLE INFO

Keywords:
Porous media
Natural convection
Lattice Boltzmann method
Darcy-Brinkman-Forchheimer model
Enclosure
Darcy number

ABSTRACT

We evaluated numerically the combined impact of Darcy and Rayleigh number changes on natural convection around two vertically arranged hot porous cylinders of different diameters in a square enclosure. Numerical simulations are conducted by implementing lattice Boltzmann technique using the D_2Q_9 model. The Darcy-Brinkman-Forchheimer equations for porous medium are solved with a single-domain approach. The influence of Darcy number ($10^{-6} \leq Da \leq 10^{-2}$) on rate of heat transfer from cylinders is described for $10^4 \leq Ra \leq 10^6$ by altering the cylinder diameter from 0.1 to 0.4*L*. With increment of cylinder size, *Ra* and *Da*, heat transfer rates are found to improve. At $Ra = 10^6$, the highest enhancement occurs for $D = 0.1$L. On lower Rayleigh numbers ($Ra = 10^4$) as well as Darcy numbers ($Da = 10^{-6}$), doubling the diameter of the cylinder increases heat transport by 41.5%. Consequently, when the diameter is multiplied by four, the improvement is 211%. At $Ra = 10^6$, the rate of augmentation from $D = 0.2$L–0.3L is lower than for the case when $D = 0.1L$ and 0.2*L*. At $D = 0.4L$ maximal transfer of heat arises when the cylinder is extremely permeable (i.e., $Da = 10^{-2}$). This study has applications in the thermal management of a bank of electronic components.

Nomenclature

Notations

C_1, C_2	Binary constants
c_F	Non-dimensional Forchheimer term
c_s	Speed of sound [ms^{-1}]
Da	Darcy number $\frac{K}{D^2}$
d_p	Particle diameter [m]
e_i	Discrete lattice velocity in direction i, $\frac{\Delta x_i}{\Delta t}$
F	Body force due to presence of the porous medium [N]
F_i	Total force term due to porous medium [N]

* Corresponding author.
E-mail address: sdhina@iiti.ac.in (S. Dhinakaran).

https://doi.org/10.1016/j.csite.2023.102907
Received 12 January 2023; Received in revised form 7 March 2023; Accepted 12 March 2023
Available online 13 March 2023

F_b	Boussinesq force term [N]
g	Gravitational acceleration [ms^{-2}]
f_i	Particle distribution function along i^{th} link direction
f_i^{eq}	Equilibrium distribution function along i^{th} link direction
g_i	Temperature distribution function along i^{th} link direction
g_i^{eq}	Equilibrium distribution function of temperature i^{th} link direction
L	Length of enclosure [m]
D	Diameter of Cylinder [m]
δ	Distance from centre (δx or δy in x and y direction)
G	Body force due to gravity [N]
N	Number of lattices on the cylinder
Nu	Local Nusselt number $\frac{\partial\theta}{\partial n}$
Nu_{Mean}	Nusselt number $\frac{hL}{K}$
p	Dimensionless pressure $\frac{p*}{\rho u_\infty^2}$
Pr	Prandtl number $\frac{\nu}{\alpha}$
Ra	Rayleigh number $\frac{g\beta\Delta TL^3}{\alpha\nu}$
u	non-dimensional x-component velocity [ms^{-1}]
v	non-dimensional y-component velocity [ms^{-1}]
U	Actual velocity [ms^{-1}]
V	Auxiliary velocity [ms^{-1}]
w_i	Weighing factor in direction i
x,y	Non-dimensional horizontal & vertical coordinate
x^*,y^*	Dimensional horizontal & vertical coordinate

Greek symbols

ρ	Fluid density [kgm^{-3}]
τ	Dimensionless relaxation time for density
τ'	Dimensionless relaxation time for temperature
t	Non-dimensional time $\frac{t*u_\infty}{H}$
Δt	Time step [s]
Δx	Lattice space
θ	Dimensionless temperature $\frac{T-T_\infty}{T_w-T_\infty}$
ε	Porosity
ν	Fluid kinematic viscosity [m^2s^{-1}]
μ	Fluid dynamic viscosity [Nsm^{-2}]
Λ	Viscosity ratio, $\frac{\mu_e}{\mu}$
α	Thermal diffusivity [m^2s^{-1}]
β	Thermal Expansion Coefficient $\frac{Ra\,\alpha\,\nu}{g\Delta TL^3}$ [K^{-1}]
σ	Thermal Conductivity ratio

Subscripts

avg	Average
∞	Far field value
$\circ$	Inlet value
Mean	Mean value
i	Lattice link direction
w	Wall
e	Effective
f	Fluid

Superscripts

$*$	Dimensional form of variables

1. Introduction

Modern technology cannot be imagined without electronic devices. Every high-tech piece of equipment around us is based on electronic chips with microprocessors. The continuous working of stationary devices generates heat which hampers their overall

efficiency. Maintaining a sufficiently low temperature is required to work efficiently. This problem leads to the emergence of research in the flow and heat transfer domain. Natural convective heat transfer has been an impressive research area for decades as its application include design of nuclear reactors, heat exchangers, electronic component cooling as well as solar panels.

Also, porous bodies are highly researched these days as it has an eminent role in heat transfer [1]. The present numerical analysis primarily examines heat transferred naturally through convection in an enclosure comprising two heated porous cylinders placed vertically. The investigation is performed by varying the cylinders' diameter and observing transitions in heat dissipation.

Natural convective heat transfer in enclosures is recognized by researchers for its fundamental and practical applications. Shruti et al. [2] conducted numerical investigation on convection occurring naturally from an enclosure containing a porous cylinder. The cylinder's position in the enclosure is shifted to top, centre, bottom, right, bottom-diagonal and top-diagonal. They found that cylinders placed at the bottom-diagonal position have a maximum rate of heat transfer. Alsabery et al. [3] examined a cavity containing solid square cylinder and Al_2O_3 - H_2O nanofluid utilising a two-phase model by Buongiorno. The solid-block size (0.1–0.7) and ratio of thermal conductivity (0.28, 0.76, 1.95, 7 and 16) affects the heat dissipation efficiency of a partly cooled and partially heated cavity. Moukalled and Acharya [4] investigated a circular cylinder heated isothermally in a closed cavity. The cylinder radius varies from 0.1L to 0.3L. In the natural convective heat transfer analysis the authors found that conduction effects are more substantial for a lower Rayleigh number of 10^4. The increment in Rayleigh number leads to more prominent convection effects, proceeding to faster heat transfer rates. Also, separation of thermal boundary layer occurs in the area over the cylinder when R/L ratio is 0.3. Roychowdhury et al. [5] studied convection by buoyancy forces inside the inner cylindrical shell using variable boundary conditions for temperature. Vertical walls, insulated and heated have also been studied with a cold cylinder inside the enclosure. When the Prandtl number is 10, the Nusselt number increases. Also, thermal stratification is noticed at enclosure aspect ratio 4 and 5. Nabavizadeh et al. [6] analysed natural convection by a sinusoidal cylinder. The undulations as well as amplitudes over the cylinder surface are changed. On increasing undulations value within range 0.4–0.8, reduction in Nusselt number is seen because of hindrance in fluid recirculation inside the gaps over the curved surface. Adding undulations of more than eight forms a circular shape, and the Nusselt number improves.

An investigation of heat transfer in an enclosure having a thermally conductive cylinder and differentially heated walls is conducted by Jami et al. [7]. As the temperature difference rises, the heated walls' mean Nu value decreases, while an inverse pattern is observed in cold walls. An extension of this study by Jami et al. [8] examined the implications to heat dissipation when cylinder position is changed in enclosure. The ratio of temperature difference between cylinder and walls is 0 and 50. At a temperature difference value 0, heat dissipates at a higher rate in the region nearby central position. Kim et al. [9] analysed thermal transfer with a cylinder placed at several locations in a cold closed cavity when Ra is between 10^3 and 10^6. The profiles of local Nusselt numbers are observed to be symmetric for various vertical positions in case of $Ra = 10^3$ and 10^4. The minimum Nu_{Mean} value is obtained in case of centre location. An analogous investigation is experimentally conducted by Hussain and Hussein [10] with a uniformly heated cylinder. The generation of thin boundary layer occurs as liquid flows near the horizontal enclosure walls. Yoon et al. [11] examined heat transfer by free convection from a cylindrical body in a closed cavity for $Ra = 10^7$. The authors observed that streamlines change as the position of the cylinder varies, specifying a transformation to an unsteady state. The flow and heat transfer rate were unchanged when the location of the cylinder ranged from 0.05 to 0.18 units beneath the centre. Analogous research by Kang et al. [12] has explored heat transfer in the case of heated cylinders located along transverse and diagonal lines in an enclosure. The study presents a series of Benard cells that control flow instability at the corners and centres of the enclosure.

Porous media has also been an important topic in research due to its impact on efficient heat transfer. Nithiarasu et al. [13] explored a porous enclosure having vertical hot and cold walls. The permeable region has uniform or variable porosity (0.4–0.9) at $Ra = 10^3$ - 5 $\times$ 10^9. According to the results, the thickness of the permeable layer affects the streamlines and isotherms. Vijaybabu [14] studied transfer of heat from CuO - H_2O nanofluid filled cavity containing a porous cylinder. The nanoparticle volume fraction and permeability varied, and its effect was investigated. It has been found that the site of the highest entropy is influenced by permeability. Hu and Mei [15] studied entropy generation in rectangular closed cavity joined to porous wall. The Nu_{avg} augments by 90% when the Darcy number increments. The efficiency of transmitting heat is reduced by up to 50% in the case of thicker porous walls. At a 90° inclined enclosure, a minimum heat transfer rate is achieved.

However, experimental and numerical research works with pairs of cylinders are also found in the literature. These studies have applications in the design of process heaters (Yoon and Jung [16], Yonco and Batta [17], Yoon et al. [18]). Yoon and Jung [16] have studied free convection in an enclosure having cold walls and two hot cylinders. Effect of cylinder radius (0.05L–0.2L) on flow and heat transfer is analysed. On enlarging cylinder radius, thermal contours in the area between two cylinders become coarser, filling the region with hotter fluid. In addition, the surface Nu_{Mean} on each enclosure wall rises with the increase in radius of cylinders. When $Ra = 10^5$, with a smaller radius of the cylinders, the symmetry inside the enclosure is distorted. Yonco and Batta [17] investigated heat transfer from two hot cylinders which are aligned vertically. The outcome states that the bottom cylinder's Nusselt number is similar to the case of one cylinder. When space between two cylinders is nine times the diameter, top cylinder's Nusselt number increases 1.5 times compared to the case where the gap is twice the diameter.

The study on two differentially heated cylinders by Yoon et al. [18] shows that a cold upper cylinder increases the region for more heat transfer in the enclosure's upper section. In an instance with a smaller radius (0.05L) cylinder, the role of convection in enhancing the Nu_{Mean} the upper cylinder overcomes conduction. In contrast, for larger sizes (0.2L), conduction effects are more substantial than convection. Sparrow and Niethammer [19] performed an experimental evaluation of heat transfer with a horizontally aligned pair of cylinders. The Nu of top cylinder enhances by a factor of 1.25, in cases of the distance between cylinders of 6–9 diameters compared to a single cylinder case. Corcione [20] studied transfer of heat from hot cylinders arranged in a vertical fashion. The heat dissipation from the cylinders placed downstream enhances or decreases depending on the location as well as separation distance within two

cylinders. The space between cylinders influences the array's overall rate of heat transfer.

Chae and Chung [21] experimentally dealt with the heat transfer by a pair of cylinders where the pitch-to-diameter(P/D) ratio varies from 1.02 to 9. The Nusselt number ratio of the top and bottom cylinder increases. In case of laminar flows, when the P/D ratio is less than 1.5, the Nusselt number ratio is less than unity, whereas, for turbulent flow, it is almost equal to 1 when P/D is near 1. An analogous experimental study was conducted by Reymond et al. [22] on a single and a pair of copper cylinders mounted horizontally inside a water tank. A bottom unheated cylinder does not influence the heat release rate of the top heated cylinder. Moreover, when both cylinders are heated, plumes rising above the bottom cylinder interact with the top cylinder plumes. The oscillating plumes from the lower cylinder can be noticed intensifying mixing and enhancing heat transfer rate.

Lacroix [23] investigated a rectangular cavity containing a pair of hot cylinders. The authors fixed the position of the bottom cylinder but varied the upper cylinder location (2.5L, 3.5L and 4.5L from the bottom). For $Ra < 10^5$, the cylinder position when the distance between cylinders is 4.5L, width 1.5L and 2L provide better heat transfer rates. The configuration with a width of 2L and the upper cylinder position at 2.5 and 3.5 has a maximum cooling rate. In addition, Lacroix and Joyeux [24] varied thermal conductivity ratio of wall and fluid along with wall's dimensionless thickness. The study further focused on the conduction in vertical walls and convection by fluid in the cavity, stating that the coupling effect within the fluid and solid wall strongly affects heat dissipation.

Park et al. [25] conducted a heat transfer analysis with single and two hot cylinders at a distance of 0.35L numerically. The upper position cylinders' local Nusselt number is less than the lower one due to more vital buoyant forces near the bottom wall. Park et al. [26] conducted a natural convection study with a cooled enclosure containing two horizontally placed cylinders at several positions. They found that the flow transformation to an unsteady regime depends on the distance between the enclosure centre and the cylinder. At $Ra = 10^6$, and separation distance of the cylinder centre from the enclosure centre is between 0 and 0.1, the flow as well as thermal fields are steady. Park's [26] study was continued further by Cho et al. [27] for two cylinders placed horizontally, vertically and diagonally. For $Ra = 10^6$, flow and temperature fields are in an unsteady regime when distance between cylinders is 0.1L in horizontal, 0.1L and 0.2L in diagonal directions, as stronger convective interactions are found in these cases.

Goswami et al. [28] numerically examined the influence of separation distance (0.1L–0.4L) within two cylinders. With increase in distance, time-averaged Nusselt number increases when $Ra = 10^4$, while for $Ra = 10^5$ and 10^6, the value increases to peak value, then reduces to lowest value and rises further. However, the enhancement rate in the Nusselt number declines for $Ra = 10^6$. Pal et al. [29] conducted an unsteady natural convection investigation with a magnetic field in a closed cavity having a working fluid of $Pr = 6.58$. The authors varied the dimensionless spacing (0.1L–0.5L) between the cylinders and noticed at higher Ra (10^6), time-averaged Nusselt number reduces when distance grows from 0.1L to 0.2L. However, they observed a slight increment with a further increase in the distance. Moreover, Seo et al. [30] numerically carried out analysis with four cylinders in an enclosure. They reported a transformation to an unsteady regime for Rayleigh number 10^6 and horizontal distance 0.3L. The instability in flow primarily affected transfer of heat in the vicinity of the top wall.

Further, recent studies with porous medium are discussed. The natural convection study in a porous enclosure, containing nanofluid based on Ag-MgO hybrid water is carried out by Mehryan et al. [31]. The results deduced that, increase in porosity value of porous media, aluminium foam and glass balls, raises and then declines its heat transfer rates. Hence, the total heat transfer ratio declines with an increment in porosity. Ghalambaz et al. [32] examined Nano-Encapsulated Phase Change material (NEPCM) inside a permeable enclosure. The unsteady natural convection flow analysis states, when NEPCM particles' volumetric concentrations exceed 3%, the increase in porosity greatly enhances heat transfer. Also, the rise in Darcy number enhances heat flow by easing the flow in pores and thus increasing convection. The mixed convection analysis by Ghalambaz et al. [33] investigated the vertical plate, immersed in permeable medium, with the NEPCM suspension. It is inference from outcomes that adding NEPCM particles leads to enhancement in heat transfer. The depletion in fusion temperature of NEPCMs, enhances surface temperature gradient along with Nusselt number over the plate. Further, Ghalambaz et al. [34] examined free convection by NEPCM in an inclined permeable enclosure having vertical heated and cold walls. The optimal thermal performance is achieved at 42° inclination angle. In presence of NEPCM particles, heat transfer enhances by 13%.

Hosseinzadeh et al. [35] studied convection heat transfer from hybrid nanofluid ($Fe_3O_4 - Al_2O_3$) along with MHD inside a wavy star-shaped porous enclosure. The outcomes suggest that porosity value 0.1 is optimum and increasing the value results in reduction of convective heat transmission rate. Selimefendigil et al. [36] showed effectiveness of utilising four porous cylinders along with inclined magnetic field and hybrid nanofluid in a vented cavity. The radius of cylinders is varied from 0.04 H to 0.15 H (H is cavity height). When permeability is lowest, using the largest cylinder size can improve heat transfer by up to 88% compared to using the smallest size, whereas it only improves it by 15% in the case of the highest permeability.

Fedotov et al. [37] studied free convection from thin layer formed within coaxial cylinders. The analysis is done for two dimensional as well as three dimensional cylinders. At Rayleigh numbers 4×10^4 and 4×10^5, the Nusselt number attained from the two dimensional analysis overstated Nu produced with three dimensional investigation by 5% and 47%, respectively. Chordiya et al. [38] determined effects of partition length on heat transfer occurring naturally within a permeable enclosure that has been heated differentially. The partitions with L-shap are efficient in minimising heat transfer rate for small size partitions (longitudinal length $B < 0.5$), whereas square-wave-shape are recommended for bigger partitions ($B > 0.5$). For the completely partitioned porous enclosure, the highest reduction is attained. Tayebi et al. [39] investigated nanofluid double-diffusive magneto-natural convection within the cavity having a wavy permeable cylinder and under local thermal non-equilibrium (LTNE) conditions. It is reported that the mass transfer rate is less sensitive than heat transfer rate to variations in permeable medium's properties. Javed et al. [40] investigated conjugate natural convection inside permeable chamber of dome shape equipped with a solid cylinder, water and permeable material of soda-lime-silicate glass bends. In order to improve heat transfer at $Ra \geqslant 10^6$, the smallest solid cylinder (0.2L), situated at the top dome plays crucial role. As the diameter increases further, diffusion dominantes when cylinder is placed close to hot wall at $Ra < 10^6$.

Reddy et al. [41] examined an inclined permeable annulus. The MHD convective analysis with $Ag - TiO_2$ hybrid nanofluid and internal heat generation shows that increment of Da significantly augments flow circulation and enhances heat transmission regardless of other parametric variables. The three dimensional analysis of free convection by nanofluid inside permeable wavy enclosure exposed to magnetic field is being conducted by Abderrahmane et al. [42] The rise in Da from 10^5 to 10^2 improved Nu_{avg} by 177% while increase in Ha from 0 to 100 decreased it by 23% at Ra = 10^6.

There are several studies on heat transfer through buoyancy-induced convection in an enclosure having heated solid cylinders (one or two) of various shapes. The flow and temperature fields in the single cylinder research are exclusively dependent on the interaction of the hot cylinder and the exterior wall of the cold enclosure. In the scenario of two hot cylinders, mutual interaction amongst heated cylinders has an added influence on flow and heat transfer [25]. The current numerical investigation is carried out by placing two porous cylinders into the enclosure. To the best of our knowledge, there is no study on the free convection of two permeable cylinders inside cooled enclosure, including the influence of their diameter. This study attempts to fill that void. The objective is to investigate the consequences of cylinder size, *Ra* and *Da* on flow and thermal characteristics and to find the optimal size of the permeable cylinder for maximal heat transmission. The numerical analysis is conducted by implementing the lattice Boltzmann method. The investigation mainly focuses on the dynamics of convection currents and heat dissipation from enclosure. This study can be used to manage a bank of electronic components' thermal performance.

2. Mathematical model

2.1. Problem statement and geometrical configuration

We conducted a computational analysis on heat transfer through natural convection, by a pair of hot porous cylinders, arranged vertically in an enclosure. The computational domain considered for this study is represented in Fig. 1. The cylinders inside the enclosure are heated isothermally (T_h) while the walls of the enclosure are cooled isothermally (T_c). The transfer of heat through cylinders is evaluated for four different sizes. The diameter of the cylinder varies between 0.1L and 0.4L in steps of 0.1. The separation distance of cylinders is kept constant (0.5L). The enclosure is filled with air whose Prandtl number is assumed to be 0.71.

To simplify the problem, we made the following assumptions:

- The flow is 2D, laminar, steady as well as incompressible.
- The properties of Newtonian fluid (air) are constant.
- Radiation effects from the cylinders are insignificant.
- Permeability and porosity of the porous media are uniform.
- The porous cylinders are isotropic and homogeneous and single-phase fluid passes through them.
- Local thermal equilibrium exists between the surrounding fluid and porous material.
- Thermal conductivity ratio between porous substance and fluid is taken as one.

2.2. Governing equations

The following dimensionless equations (Darcy-Brinkman-Forchheimer model) describe heat transfer by natural convection from porous cylinders inside a 2D square enclosure [13]:

$$\frac{\partial u}{\partial x}+\frac{\partial v}{\partial y}=0 \tag{1}$$

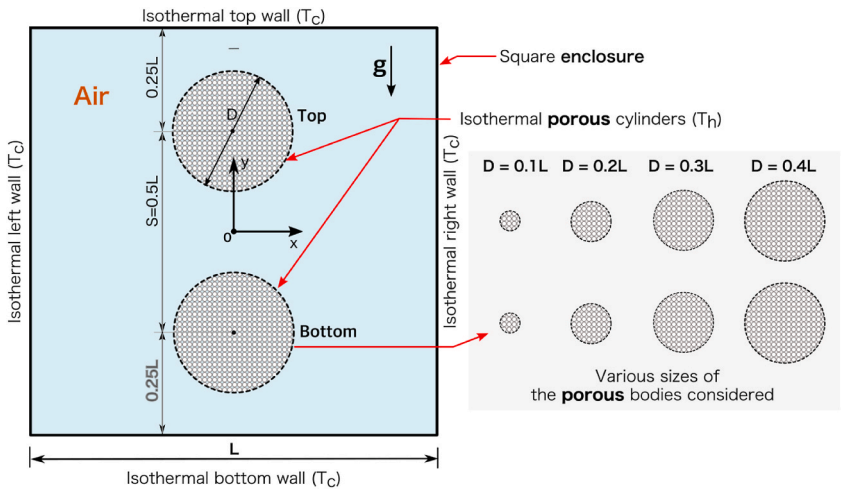

Fig. 1. Sketch of the computational set-up. Different cylinder sizes considered are shown on the right.

$$\frac{1}{\varepsilon}\frac{\partial u}{\partial \tau_t}+\frac{1}{\varepsilon^2}\left(u\frac{\partial u}{\partial x}+v\frac{\partial u}{\partial y}\right)=-\frac{\partial p}{\partial x}+\frac{Pr}{\varepsilon}\left(\frac{\partial^2 u}{\partial x^2}+\frac{\partial^2 u}{\partial y^2}\right)-C_1\frac{Pr}{Da}u-C_2\frac{1.75}{\sqrt{150}}\frac{1}{\sqrt{Da}}\times\frac{\sqrt{u^2+v^2}}{\varepsilon^{3/2}}u \tag{2}$$

$$\frac{1}{\varepsilon}\frac{\partial v}{\partial \tau_t}+\frac{1}{\varepsilon^2}\left(u\frac{\partial v}{\partial x}+v\frac{\partial v}{\partial y}\right)=-\frac{\partial p}{\partial y}+\frac{Pr}{\varepsilon}\left(\frac{\partial^2 v}{\partial x^2}+\frac{\partial^2 v}{\partial y^2}\right)-C_1\frac{Pr}{Da}v-C_2\frac{1.75}{\sqrt{150}}\frac{1}{\sqrt{Da}}\times\frac{\sqrt{u^2+v^2}}{\varepsilon^{3/2}}v+Ra\ Pr\ \theta \tag{3}$$

$$\sigma\frac{\partial \theta}{\partial \tau}+\left(u\frac{\partial \theta}{\partial x}+v\frac{\partial \theta}{\partial y}\right)=\frac{k_{eff}}{k_f}\left(\frac{\partial^2 \theta}{\partial x^2}+\frac{\partial^2 \theta}{\partial y^2}\right) \tag{4}$$

The Prandtl number, $Pr=\mu C_p/k_f$. C_1 and C_2 are binary constants. The value of C_1 is defined as 0 for the fluid region, and C_2 is equal to 1 for the permeable zone. The thermal properties of fluid and porous medium are presumably similar, hence $\sigma=1$ and $k_{\text{eff}}=k_{\text{f}}=k_{\text{s}}$. The effective thermal conductivity is determined as [44]

$$k_{eff}=\varepsilon k_f+(1-\varepsilon)k_s \tag{5}$$

The ratio of thermal conductivity (σ), of fluid and permeable medium and is assumed as 1 to emphasise the flow effects due to heterogeneous porosity variation [13].

The dimensionless equations are expressed with the following characteristic scales:

$$x=\frac{x^*}{L},y=\frac{y^*}{L},u=\frac{u^*L}{\alpha},v=\frac{v^*L}{\alpha},p=\frac{p^*L^2}{\rho\alpha^2},\theta=\frac{T-T_c}{T_h-T_c} \tag{6}$$

In the above equation, the superscript * represents the dimensional variable.

The following equation evaluates the local Nusselt number (Nu) along enclosure walls:

$$Nu=-\frac{\partial T}{\partial n} \tag{7}$$

Here, n denotes normal coordinate to wall's surface. Numerical integration of local Nusselt number values of the enclosure walls is carried out to obtain the mean Nusselt number as

$$Nu_{Mean}=\frac{1}{L}\int_0^L Nu\,dL \tag{8}$$

Here, L represents the length of each wall. Nu is calculated on all enclosure walls, and then the mean (Nu_{Mean}) is evaluated.

2.3. Lattice Boltzmann Method

The numerical investigations are done with the mesoscopic approach termed as Lattice Boltzmann Method. The analysis is carried out in a computational domain, divided into lattices. Further, collision and streaming occur in each lattice. Along with these steps, parameters including density, velocity, and temperature have been evaluated for each domain lattice. In the equations of LB,

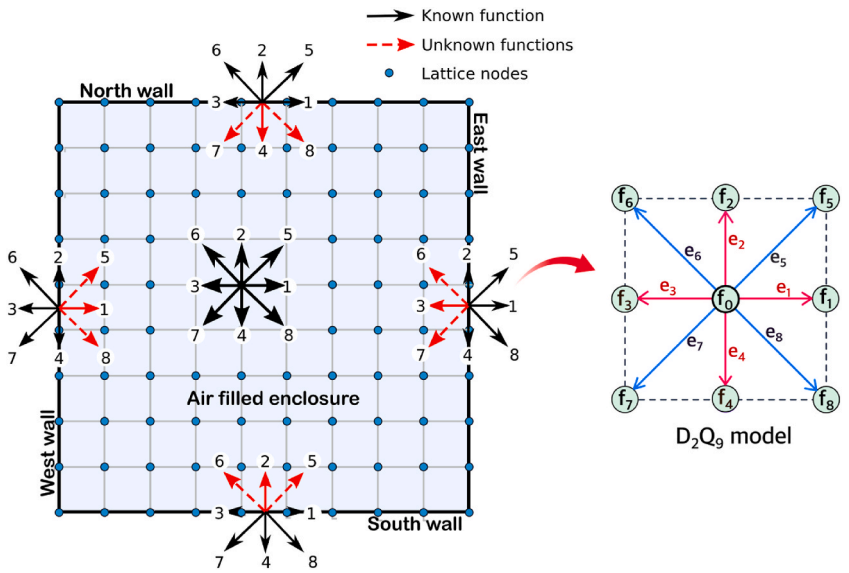

Fig. 2. Lattice structure, boundary treatment for D_2Q_9 lattice [46] and the configuration of lattice in D_2Q_9 model along with the velocity vectors [29].

convection terms are linear, whereas the Navier-Stokes equation terms are non-linear.

2.3.1. Lattice Boltzmann equation for flow domain

The initial step is collision. Collisions between particles must occur at every node before streaming. The equation for collision step is expressed as [45].

$$f_i(x+e_i\Delta t, t+\Delta t) - f_i(x,t) = -\frac{1}{\tau}[f_i(x,t) - f_i^{eq}(x,t)] + \Delta t F_b + \Delta t F_i \tag{9}$$

In the above equation, f_i represents the instantaneous velocity of the particles, f_i^{eq} corresponding equilibrium density along with e_i showing vector direction of particle velocity within the lattice. F_i accounts for force term, due to presence of permeable body, and F_b represents the force term due to natural convection effects.

A two-dimensional numerical study is performed by using the D_2Q_9 model (Fig. 2). The particle's velocity are represented as [45].

$$e_i = \begin{cases} (0,0), & i = 0 \\ (\cos[(i-1)\pi/2], \sin[(i-1)\pi/2])e, & i = 1-4 \\ (\cos[(2i-9)\pi/4], \sin[(2i-9)\pi/4])\sqrt{2e} & i = 5-8 \end{cases} \tag{10}$$

In Eq. (9), the initial term on right side represents a single relaxation time (SRT) BGK collision operator. At every collision step, the particles relax to equilibrium. The value of the relaxation factor (τ) is uniform for each particle in all lattices. The mathematical statement relating the viscosity of the fluid in Lattice Boltzmann to its non-dimensional relaxation time is given by the Chapman-Enskog equation. The expression is as follows [45]:

$$v = \left(\tau - \frac{1}{2}\right)\Delta t\, c_s^2 \tag{11}$$

Eq. (9) is appended to the force term F_i accounts for the influence of drag/viscous resistance force induced by the permeable region. As fluid passes across permeable medium and experiences viscous resistance. In the fluid region without porous medium, this force term is specified at a value 0 which further nullifies its effect. However, in a porous region, the force term is calculated as shown in Eq. (12). In the current study, D_2Q_9 model is used, where $c_s = \frac{c_k}{\sqrt{3}}$, c_s represents the speed of sound [45] and the equation for F_i is given as

$$F_i = w_i\rho\left(1 - \frac{1}{2\tau}\right)\left[3(e_i\cdot F) + \frac{9}{\varepsilon}(e_i\cdot U)(e_i\cdot F) - \frac{3}{\varepsilon}(U\cdot F)\right] \tag{12}$$

The force due to the porous region is both viscous and inertial, termed as Darcy-Forchheimer force denoted by F. This force term is expressed as [43].

$$F = -\frac{\varepsilon v}{K}U - \frac{\varepsilon c_F}{\sqrt{K}}|U|U + \varepsilon G \tag{13}$$

In the above equation, ε is porosity, K denotes permeability of porous region, v refers to fluid kinematic viscosity, the dimensionless Forchheimer term $c_F = 1.75/\sqrt{150\times\varepsilon^3}$, and $|U| = \sqrt{u^2+v^2}$. Here, u and v represent velocity components in x and y directions. G refers to body force caused by gravity. Further, equation relating the porosity and updated equilibrium distribution function is given as follows [43]:

$$f_i^{eq} = w_i\rho\left[1 + 3(e_i\cdot U) + \frac{9}{2\varepsilon}(e_i\cdot U)^2 - \frac{3}{2\varepsilon}(U\cdot U)\right] \tag{14}$$

In the lattice arrangement, w_i denotes the weighing factor for every lattice. The weighing factor values in the D_2Q_9 model are $w_o = 4/9$, $w_i = 1/9$ ($i = 1$–4), $w_i = 1/36$ ($i = 5$–8). Collision, streaming, then implementation of appropriate boundary conditions are carried out at meso-level. Subsequently, the macroscopic parameters are evaluated. Summation of the distribution function values at every lattice node corresponds to the fluid density at that particular point. However, the fluid's velocity (U) and density (ρ) can be obtained through values of the distribution function as mentioned in the following equations [45]:

$$\rho = \sum_{i=0}^{8} f_i \tag{15}$$

The variable V in Eq. (16), represents the auxiliary velocity, which arises due to permeable region.

$$\rho V = \sum_{i=1}^{8} e_i f_i + \frac{\Delta t}{2}\rho F \tag{16}$$

The actual velocity inside porous media is calculated with this expression:

$$U = \frac{V}{c_0 + \sqrt{c_0^2 + c_1|V|}} \tag{17}$$

In above equation, parameters c_0 and c_1 are determined by

$$c_0 = \frac{1}{2}\left(1 + \varepsilon \frac{\Delta t}{2} \frac{v}{K}\right) \; ; \; c_1 = \varepsilon \frac{\Delta t}{2} \frac{c_F}{\sqrt{K}} \tag{18}$$

The collision equation is appended with an additional force term F_b accounts for natural convection. The equation for calculation of Boussinesq approximation F_b is written as [45].

$$F_b = 3 w_i g \beta \theta e_{iy} \tag{19}$$

Here, e_{iy} denotes y-direction velocity vectors.

2.3.2. Lattice Boltzmann equation for thermal domain

The temperature at each lattice is calculated with following expressions [45]:

$$g_i(x + e_i \Delta t, t + \Delta t) - g_i(x,t) = -\frac{1}{\tau'}\left[g_i(x,t) - g_i^{eq}(x,t)\right] \tag{20}$$

Here, thermal relaxation time (τ') is determined by the Chapman-Enskog equation represented as

$$\alpha = \left(\tau' - \frac{1}{2}\right) \Delta t \, c_s^2 \tag{21}$$

The following equation shows calculation of equilibrium distribution function (g_i^{eq}) :

$$g_i^{eq} = w_i \theta [1 + 3(e_i \cdot U)] \tag{22}$$

The distribution function 'g' evaluates the fluid temperature θ from the following equation:

$$\theta = \sum_{i=0}^{8} g_i \tag{23}$$

2.4. Boundary conditions

The velocity is zero, no slip ($U = 0$), and low temperature ($\theta = 0$) boundary conditions are prescribed for enclosure walls. However, a constant high temperature ($\theta = 1$) is imposed in the permeable zone. The boundary conditions are implemented by distribution functions (f and g) [45] as mentioned in Table 1

The following expression specifies the porous region in the computational domain:

$$\sqrt{(x - x_{cen})^2 + (y - y_{cen})^2} \leq radii \tag{24}$$

Throughout the computational field, a dummy array is specified with a value of "one" in the circular porous zone and "zero" in fluid zone. In addition, $\theta = 1$ is imposed throughout the porous domain rather than only on surface. Furthermore, $\theta = 0$ is set in clear fluid zone. The following equation describes thermal boundary conditions:

$$g_i = \theta \; * (w_i + \overline{w}_i) - \overline{g}_i \tag{25}$$

In this case, w_i denotes the weighing factor for the corresponding lattice link and $\overline{w}_i$ is the corresponding opposite link, g_i denotes the distribution function, and $\overline{g}_i$ for corresponding opposite lattice links in the thermal field.

2.5. Dimensionless parameters

In the present study, Rayleigh (Ra) and Darcy numbers (Da) are the dimensionless parameters. The value of Rayleigh number is expressed as

$$Ra = \frac{g \beta \Delta T L^3}{\nu \alpha} \tag{26}$$

Here, the characteristic height is considered in terms of the length of enclosure L. The Darcy number presents the impact of non-dimensional permeability on a region of porous medium and is given as

Table 1
Boundary conditions applied to enclosure walls while implementing LBM.

Wall	Flow	Thermal
Right	$f_3 = f_1, f_7 = f_5, f_6 = f_8$	$g_3 = -g_1, g_7 = -g_5, g_6 = -g_8$
Left	$f_1 = f_3, f_5 = f_7, f_8 = f_6$	$g_1 = -g_3, g_5 = -g_7, g_8 = -g_6$
Top	$f_4 = f_2, f_8 = f_6, f_7 = f_5$	$g_4 = -g_2, g_8 = -g_6, g_7 = -g_5$
Bottom	$f_2 = f_4, f_6 = f_8, f_5 = f_7$	$g_2 = -g_4, g_6 = -g_8, g_5 = -g_7$

$$Da = \frac{K}{D^2} = \frac{K}{N^2} \tag{27}$$

In the above equation, D denotes the permeable cylinder diameter (characteristic height), and K is the permeability. The calculation of Darcy number in terms of porosity (ε) is given by the Carman-Kozeny relation [47–49] as shown below

$$Da = \frac{K}{D^2} = \frac{K}{N^2} = \frac{1}{180}\frac{\varepsilon^3 d_p^2}{D^2(1-\varepsilon)^2} \tag{28}$$

Here, the particle diameter (0.01 m for 1 m characteristic height of porous body) is considered same to calculate Darcy number (10^{-6}, 10^{-4} and 10^{-2}). The variation in results with porosity value ranging from 0.5 to 0.9 are negligible as it has very less influence on flow [50].

3. Numerical methodology

The present heat transfer analysis is carried out utilising an in-house code based on the Lattice Boltzmann Method. Here, flow and thermal boundary conditions are modified as per the previous sections' equations. Further, the collision equation appends an additional force term due to natural convective forces. The buoyant force (F_b), including acceleration due to gravity (g), is determined by Boussinesq approximation over the whole domain. This value is in accordance with Rayleigh number. Initially, the velocity at each node in the domain is specified zero and the hot region temperature is fixed as 1. The value of $\sqrt{g\beta\Delta TL}$ must be less than or equal to 0.1 for stable solutions [45]. The calculations are terminated when subsequent convergence are reached, as shown below

$$\frac{\sqrt{\sum_{ij}\left[u_{ij}^{n+1}-u_{ij}^{n}\right]^2}}{\sqrt{\sum_{ij}\left[u_{ij}^{n+1}\right]^2}} \le 1\times10^{-5}, \frac{\sqrt{\sum_{ij}\left[v_{ij}^{n+1}-v_{ij}^{n}\right]^2}}{\sqrt{\sum_{ij}\left[v_{ij}^{n+1}\right]^2}} \le 1\times10^{-5}, \frac{\sqrt{\sum_{ij}\left[\theta_{ij}^{n+1}-\theta_{ij}^{n}\right]^2}}{\sqrt{\sum_{ij}\left[\theta_{ij}^{n+1}\right]^2}} \le 1\times10^{-6} \tag{29}$$

Here, n refers to the time step, i and j represent position of nodes, $u(i, j)$ & $v(i, j)$ are the velocities in x- and y-direction, respectively, also θ (i, j) indicates the value of temperature.

3.1. Code verification

We computed the mean Nusselt number (Nu_{Mean}) for the free convective heat transfer from enclosures using the current code developed according to the lattice Boltzmann technique. We compared the acquired findings with those available in the archival literature.

For the natural convection heat transfer with two vertically arranged solid cylinders inside enclosure, Yoon et al. [16] presented the Nu_{Mean} of the top wall for various cylinder radii, i.e., $0.05 \le R \le 0.2$ for different Rayleigh numbers. In Ref. [16], the hot circular cylinders are vertically arranged, and enclosure walls are cold.

As presented in Fig. 3 (a), our computed findings for the Nu_{Mean} are in good agreement with theirs. We observed a marginal deviation with Yoon et al. [16] as they had carried out the numerical analysis using the Immersed Boundary Method. We also validated our code with the results of Nithiarasu et al. [13] for the natural convection heat transfer inside porous enclosure. Here, the porous-filled enclosure has adiabatic upper and lower walls ($Pr = 1.0$) and side walls are differentially heated. As seen in Fig. 3(b), a good correlation exists. The results obtained by present code are observed to be within 1% of those in the literature.

3.2. Mesh dependence tests

The two-dimensional computational domain is divided into uniform grids. The solutions are obtained at various mesh sizes for

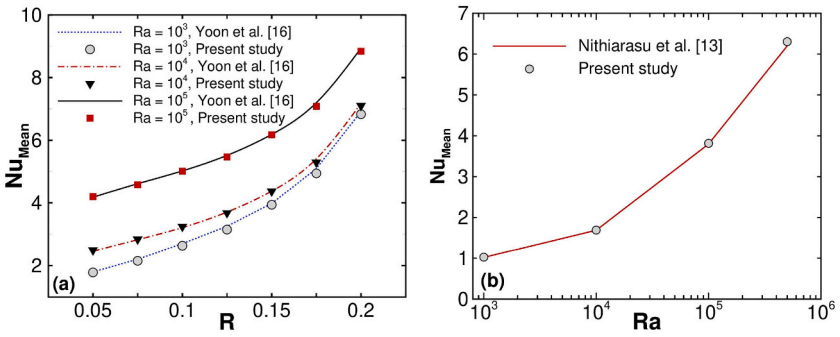

Fig. 3. Comparison of (a) Mean Nusselt number of the enclosure top wall with the literature [16] at $Pr = 0.7$ and (b) Mean Nusselt number of the enclosure with Ref. [13].

different diameters of cylinders. The lattice count on the enclosure wall (i.e., the characteristic height, L) influences the precision of the findings. The relaxation factor in the collision equation relies on the characteristic height, which is crucial for maintaining the stability of the solution. Hence, a larger number of grids provide more stable solutions with utmost accuracy. The increment in the size of the mesh decreases the rate of convergence. As a result, there's a need for optimal grid size for performing the analysis.

Fig. 4 presents the variation in the mean Nusselt number values for various mesh sizes. Test simulations were carried out with 100 × 100, 200× 200, 300× 300, 400× 400, 500× 500, 600× 600, and 700× 700 mesh sizes for $D = 0.1L$–$0.4L$ in steps of 0.1. Each lattice is of size 1. Flow and heat transfer phenomena in the vicinity of permeable regions must be captured with utmost accuracy. The intermediate parameters, $Da = 10^{-4}$ and $Ra = 10^5$, are considered for the grid-independent study. Convection has stronger impact at Ra=10^5 than it does at Ra=10^4, when conduction is the predominant mode of heat transfer [26]. The porous medium's penetrating capacity enhances at Da=10^{-4}. The outcomes are compared with a finer mesh (600 × 600).

As shown in Fig. 4, the results across 500 × 500 grids show very little change. The percentage difference between the data shown with 500× 500 grids and 600× 600 grids was less than 0.5% in Nu_{Mean}. Although the results do not vary much for grid size beyond 500 × 500, we utilised a grid size of 600× 600 to showcase the best flow features in the flow field (i.e., streamlines). Also, cartesian mesh is the sole type that can be used in the Lattice Boltzmann method. Since, two porous cylinders are investigated, that are circular in shape. Thus, mesh must be fine in order to prevent the staircase profile from capturing thermal boundary layer around the circular region. As a result, the numerical analysis is carried out using a mesh size of 600× 600 (see Fig. 4).

4. Results and discussions

The study is performed numerically to investigate the flow and thermal characteristics of an air-filled enclosure with two permeable cylinders aligned vertically using LBM. The diameter of the cylinder ranges from 0.1L to 0.4L. The effect of Darcy number, Rayleigh number as well as cylinder size on flow and heat transfer is analysed with following variations.

- Rayleigh Number (Ra) = 10^4, 10^5, and 10^6
- Darcy number (Da) = 10^{-6}, 10^{-4}, and 10^{-2}
- Porosity (ε) = 0.629, 0.977, and 0.993 corresponding to Darcy number of 10^{-6}, 10^{-4}, and 10^{-2}, respectively, calculated as per Eq. (28).

The following sections describe the results in detail.

4.1. Local Nusselt Number

The changes in Nu along the enclosure walls are shown as local Nusselt Number for $D = 0.1L$–$0.4L$. When $Ra = 10^4$, the local Nusselt number (Nu) profiles are unaffected by Darcy number (Fig. 5 (a)- (c)). The symmetric Nusselt number profiles about middle of the top (A-B) and bottom walls (C-D) are seen, hence the magnitude of Nu is maximum at the middle irrespective of size of cylinders and Darcy numbers. The Nu profiles on the sidewalls, namely, right (B–C) and left walls (D-A), are asymmetric about the middle point. Although the profiles for all Darcy numbers are similar, a close observation finds that the magnitude of local maxima changes with the Darcy number, shifting upwards at Darcy number 10^{-2}.

For Rayleigh number 10^5, when $D = 0.1L$ (Fig. 5 (d) and (e)), local maxima do not occur at the midpoints but do occur on either side of the midpoint of the top wall. This is due to heated cylinders in the middle and increased convective effects. In Fig. 5(f), a sudden jump in local maxima at $Da = 10^{-2}$ is observed when the diameter of the cylinder increases from 0.3L to 0.4L. It will be shown later in streamlines that the innermost eddy inclines towards the bottom wall, more fluid absorbs heat and flows towards the walls, and isotherms are uniform on both enclosure sides; heat transfer enhances from bottom wall as well. The magnitude of the peak increases along the side walls as well. The local maxima for side walls is attained near the bottom cylinder. For $D = 0.4L$, the parabolic shape of this profile changes at $Da = 10^{-2}$, indicating a higher Nusselt value in the middle of side walls. On raising Rayleigh number to 10^6 (Fig. 5 (g)–(i)), it is seen that for $D = 0.1$L and $Da = 10^{-2}$, local maxima move toward the side walls, but for $D = 0.4$L and $Da = 10^{-2}$, the

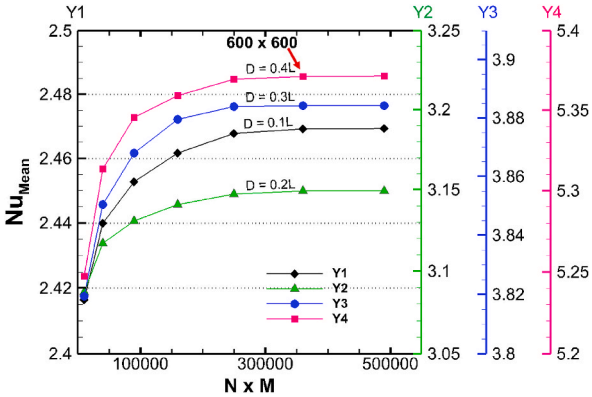

Fig. 4. Grid dependence tests carried out for various lattice size for cylinder size 0.1L ≤ D ≤ 0.4L.

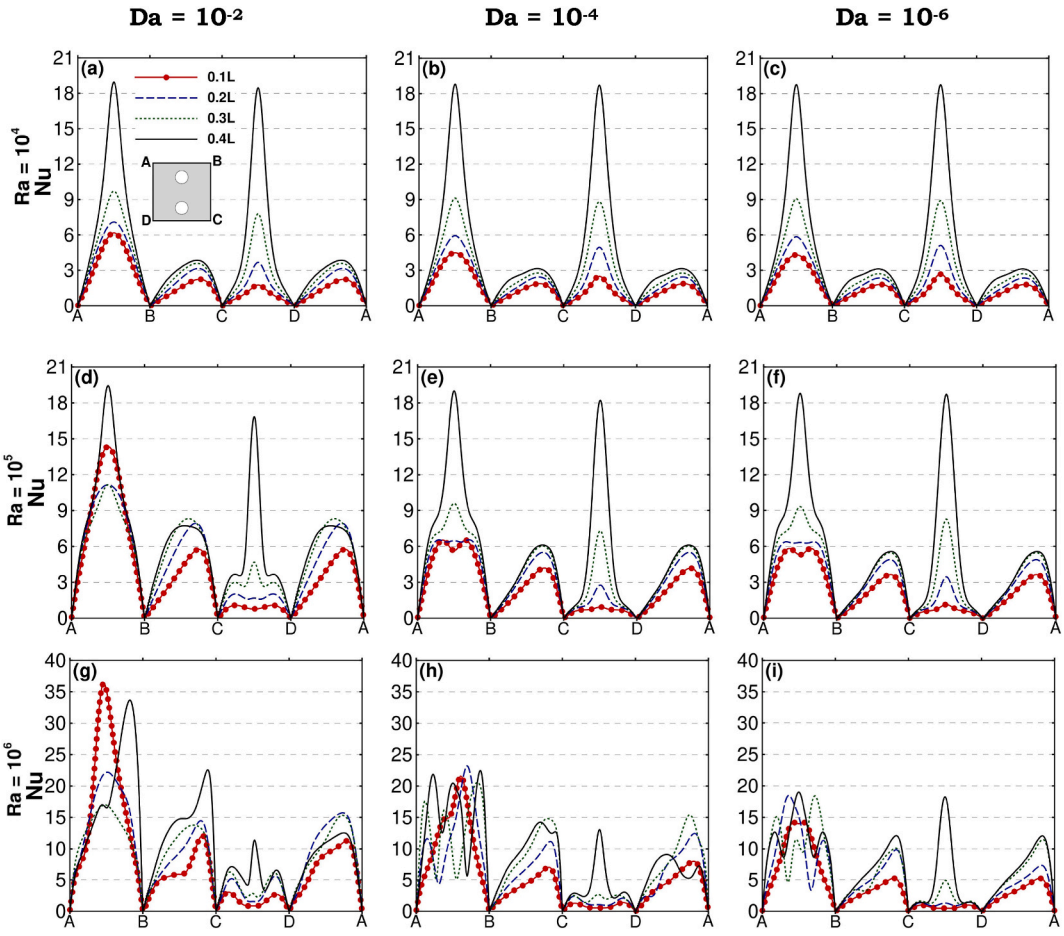

Fig. 5. The profiles of local Nusselt number along enclosure walls for various sizes of cylinders (D = 0.1L–0.4L) at $Da = 10^{-6}$, 10^{-4} and 10^{-2} when $Ra = 10^4$ (*a-c*), $Ra = 10^5$ (*d-f*) and $Ra = 10^6$ (*g-i*).

peak value is obtained in mid of top wall. The local maxima at $D = 0.3L$ are higher than that of *0.4L*. As the isotherms spread towards the walls of enclosure, heat transport is more elevated. The local maxima of the top wall for $D = 0.2L$ and *0.4L* coincides. The recirculation of heated fluid close to top wall lowers the heat dissipation through the top wall, and local Nusselt number profiles are observed to be non-uniform.

4.2. Mean Nusselt Number

When the heated cylinder's size changes from *0.1L* to *0.4L*, the influence of *Ra* and *Da* on heat transfer is noticed. In Fig. 6 (a)–(c), the Nu_{Mean} of enclosure walls is presented as a function of the diameter of porous cylinders.

When the diameter of the cylinders is *0.4L* as opposed to *0.1L*, the Nu_{Mean} of the enclosure rises for a fixed Rayleigh number. In addition, as the strength of buoyant forces grows, Nu_{Mean} rises with *Ra*. The mean Nusselt number at $Da = 10^{-6}$ and 10^{-4} for Rayleigh number 10^4 are almost equal, whereas a slight increase is seen for Darcy number 10^{-2}. The enclosure's mean Nusselt number doesn't change much when the permeability is changed because most of the forces that control how heat moves are conductive forces. When the diameter of the cylinder is doubled, the value of NuMean goes up by 41.5% at $Da = 10^{-6}$. When the diameter is made four times bigger, the improvement is 211%.

When *Ra* is raised to 10^5, buoyant forces are observed to be more prominent. This can be substantiated by the fact that the value of Nu_{Mean} rises by 38.2% for $D = 0.4L$ at $Da = 10^{-2}$ compared to the low Rayleigh value (10^4). For $Ra = 10^6$, the increment rate in Nu_{Mean} is high as a result of much stronger convective forces. At $D = 0.2L$ and $Da = 10^{-2}$, the general trend contrasts as a slight increase in value is noticed for $D = 0.3L$. Later in the streamline and thermal contours, it can also be observed that the hotter fluid circulates near top wall in case of $D = 0.2L$. In contrast, it circulates near the sidewalls as the diameter of cylinders increases to *0.4L*, thereby enhancing the mean Nusselt number.

Among all the cases studied, the maximum value of Nu_{Mean} is obtained for $D = 0.4L$ when $Da = 10^{-2}$ and $Ra = 10^6$. The space for fluid recirculation inside the enclosure reduces because of the large cylinder size. However, conductive effects enhance along with the stronger convective effects at $Ra = 10^6$.

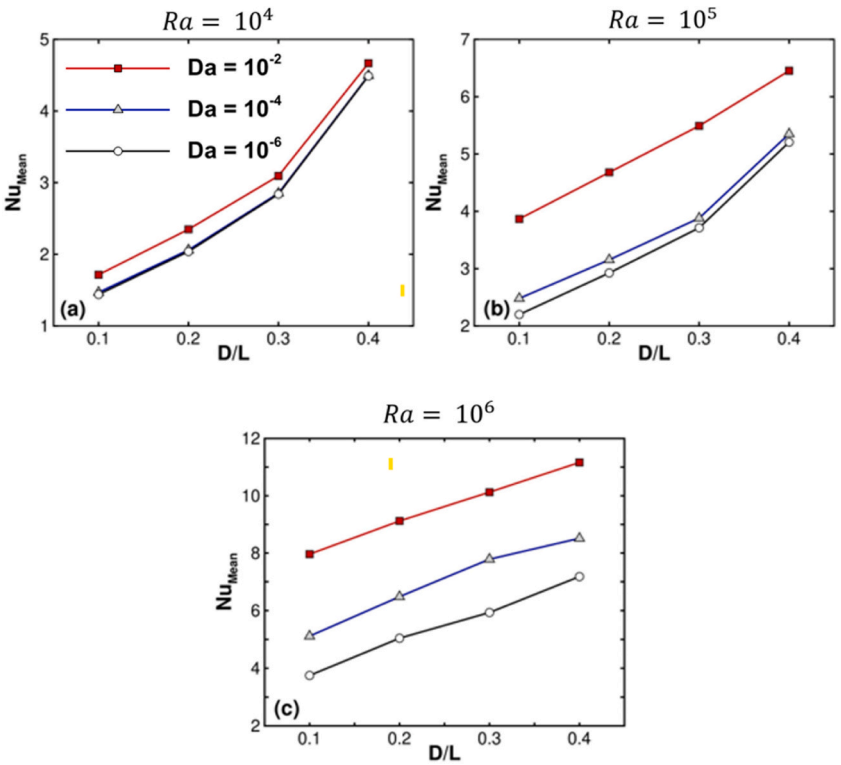

Fig. 6. Nu_{Mean} of the enclosure walls for various cylinder sizes for $Da = 10^{-6}$, 10^{-4} and 10^{-2} for (a) $Ra = 10^4$, (b) $Ra = 10^5$, and (c) $Ra = 10^6$.

4.3. Heat transfer enhancement ratio

The heat transfer enhancement ratio (ER), also known as the ratio of the Nusselt number at any Darcy number and the Nusselt number at $Da = 10^{-6}$ and is given as

$$ER = \frac{Nu}{Nu_{Da=10^{-6}}} \tag{30}$$

It describes the degree of increment in Nusselt number of the porous cylinder compared to the near-solid case (i.e., $Da = 10^{-6}$). Fig. 7 depicts variation in heat transfer enhancement ratio. When $Ra = 10^4$ and $Da = 10^{-4}$, ER for $0.1L \leq D \leq 0.4L$ is close to unity,

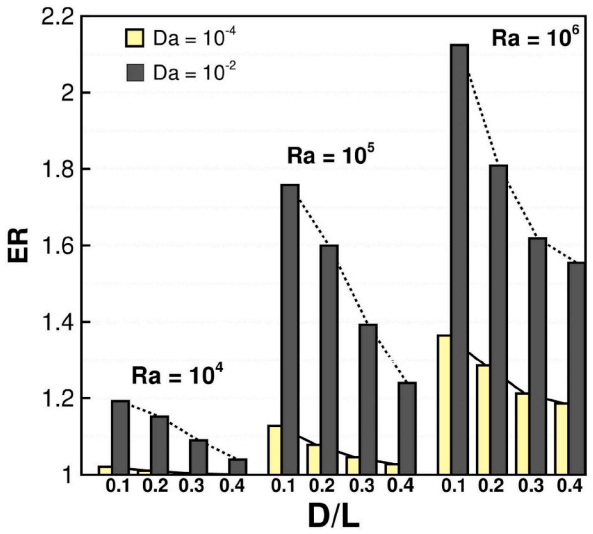

Fig. 7. Heat transfer enhancement ratio (ER) at $Ra = 10^4$, 10^5 and 10^6 for $Da = 10^{-4}$ and 10^{-2} at different sizes of cylinders ($0.1L \leq D \leq 0.4L$).

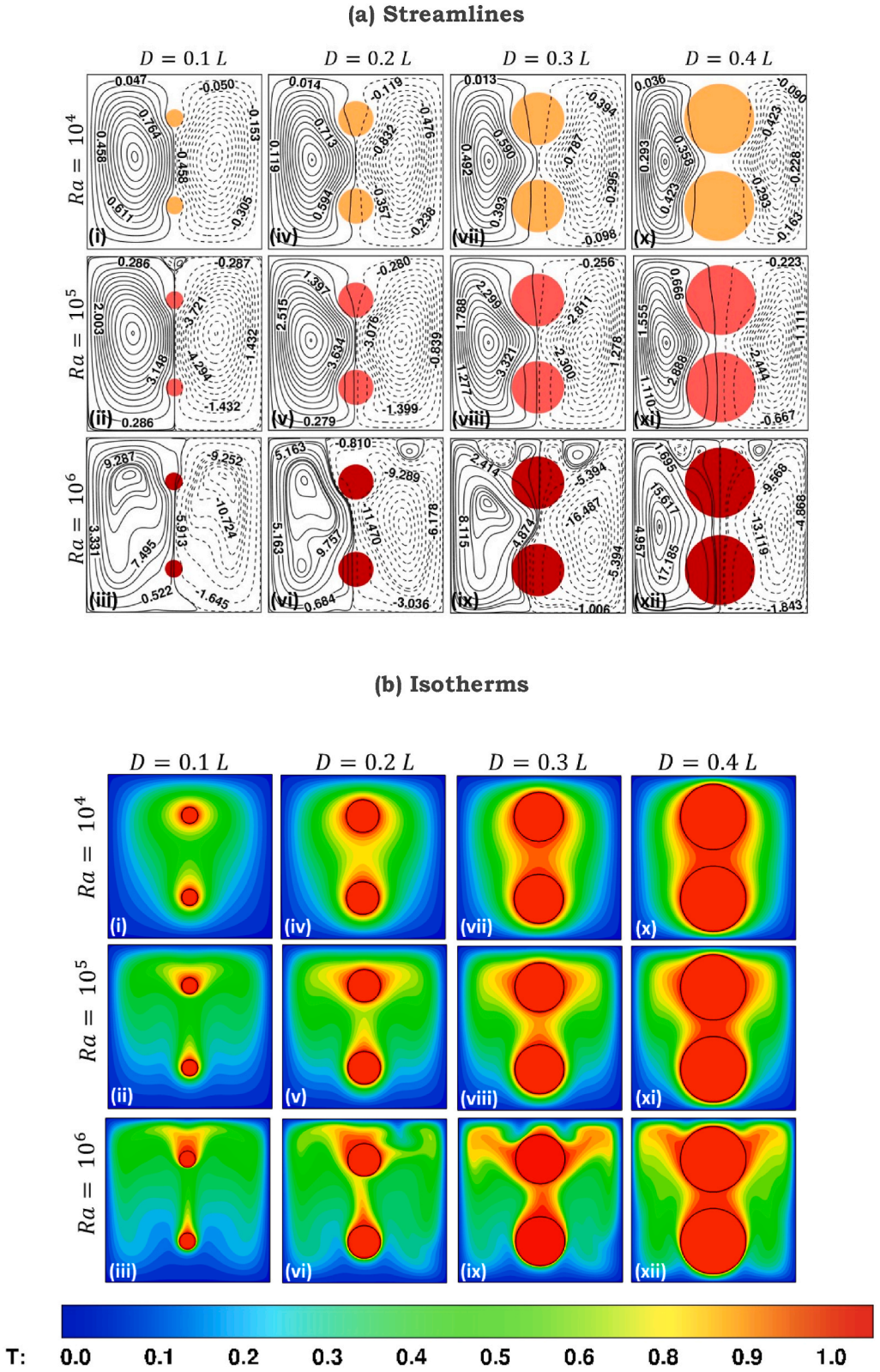

Fig. 8. **(a)**: Streamlines and **(b)** isotherms in and around the porous cylinders at $Da = 10^{-4}$, and $Ra = 10^4$, 10^5 and 10^6.

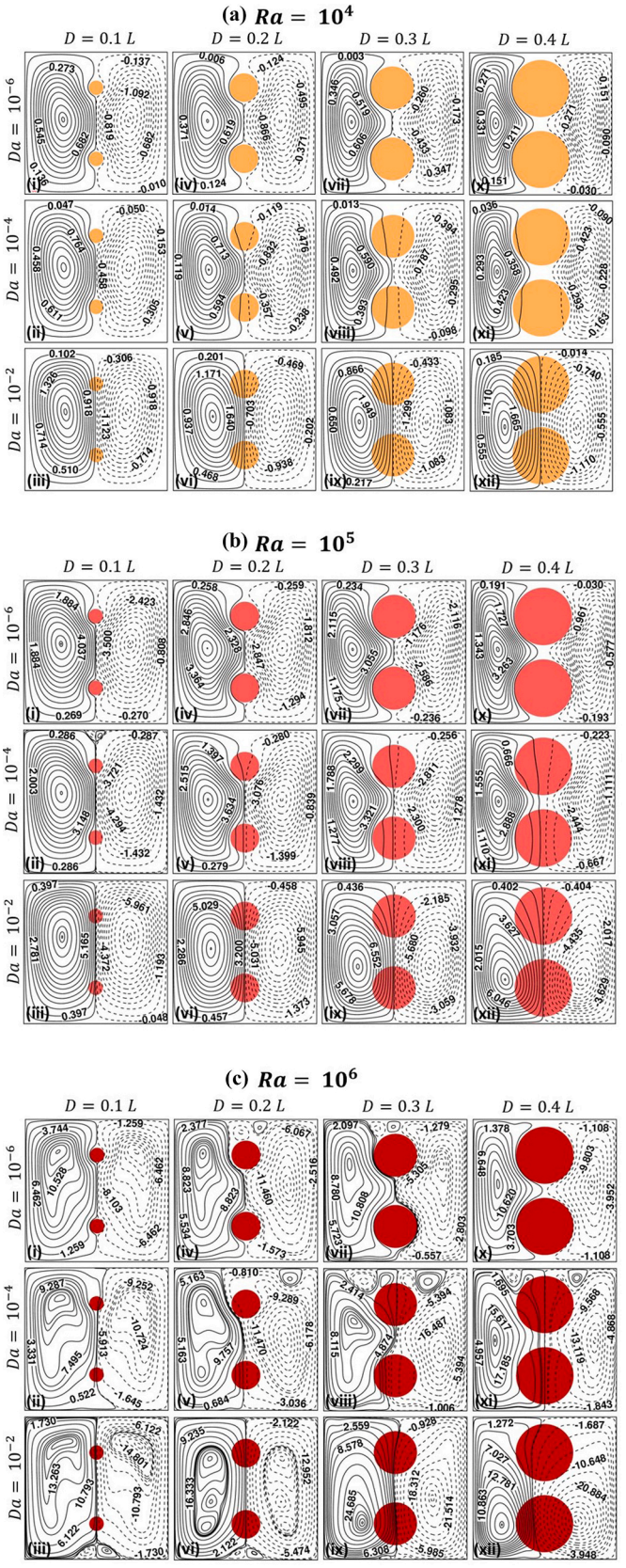

(caption on next page)

Fig. 9. Streamlines in and around the porous cylinders at (a) $Ra = 10^4$ (b) $Ra = 10^5$ and (c) $Ra = 10^6$ for $Da = 10^{-6}$, 10^{-4}, and 10^{-2}.

which means the rate of heat transfer is equal to $Da = 10^{-6}$. We observe a slight decrement in ER with an increment in cylinder size. At $Da = 10^{-2}$ and $D = 0.1L$, $ER = 1.2$. In this case, the convection forces are weak, but the heat transfer intensifies as the permeability increases at $Da = 10^{-2}$. At $D = 0.4L$, the ER gradually drops to 1.04 due to the enlarged surface area of heated bodies and reduced space for fluid circulation towards cold walls. At lower Ra values (i.e., $Ra = 10^4$), the influence of Da and cylinder size is minimal on ER. At $D = 0.1L$ and $Da = 10^{-2}$, ER rises by 20%, and a gradual decrease is observed with an increment in cylinder diameter.

On increasing Rayleigh number to 10^5, for $Da = 10^{-4}$, the enhancement ratio increases compared to $Ra = 10^4$ but does not vary much with cylinder size. In case of $Da = 10^{-2}$, ER elevates for $D = 0.1L$ as the magnitude of convective forces rises. A sudden enhancement of 70% is obtained. A steep fall is observed as the cylinders diameter increases from $0.1L$ to $0.4L$.

For a large Rayleigh number ($Ra = 10^6$), and at $Da = 10^{-4}$, the ER value is 1.35 at $D = 0.1L$, and it decreases with an increment in cylinder size. But in the case of highly permeable cylinder, i.e. when $Da = 10^{-2}$, an ER value of 2.11 is obtained at $D = 0.1L$. The sudden expansion in region for fluid flow through heated cylinders when $Da = 10^{-2}$ at $D = 0.1L$ with stronger convective effects lead to increased ER value. Further, the continuous decline in ER value with D indicates that the effects of permeability are more pronounced at $D = 0.1L$ compared to $D = 0.4L$. As the large size cylinders occupy more space inside the enclosure, the convective and conductive effects are observed.

4.4. Streamlines and isotherms

Fig. 8 (a) and Fig. 9 (a)-(c) show how the flow patterns change when Da, Ra, and the size of the cylinders change. Figs. 8(b) and 10 (a)–(c) show the isotherms around the heated porous cylinders.

4.4.1. Effect of Darcy number and Rayleigh Number

In Fig. 8, the influence of Ra variation on the streamline patterns and isotherms are shown at Darcy number 10^{-4} when the cylinder size is varied from $D = 0.1L$–$0.4L$. The buoyancy force varies with Rayleigh number.

At lower Rayleigh number, due to stronger conductive forces and weak convective forces, fluid recirculates around the cylinders. In Fig. 8(a-b)((i)(iv)(vii)(x)), for $Ra = 10^4$, small amounts of fluid entering the cylinder can be seen as a result of greater viscous resistance regardless of the size variation. However, buoyant forces increase by increasing the Rayleigh level to 10^5 (Fig. 8(a and b) (ii)(v)(viii)(xi)), thereby inducing convection effects. Hence, more fluid penetrates inside the cylinders and then recirculates, carrying heat from the heated cylinder towards the cooled enclosure wall. Heat flows towards the cold wall due to the difference in temperature between the hot cylinder and the enclosure walls. On further increasing the Rayleigh number to 10^6, convective effects augment, and symmetry of the flow field distorts for all sizes of cylinders. A large quantity of fluid flows through the lower cylinder compared to the upper cylinder, even at $Da = 10^{-4}$, which was not observed for Rayleigh number 10^4. This is due to the stronger convective forces near the bottom wall. Four eddies can be observed above the top cylinder at $D = 0.3L$ (Fig. 8 (a)(vii)-(ix)). When the cylinder diameter increases to $0.4L$ (Fig. 8(a) (x)-(xii)), the size of two eddies close to the cylinders reduces, indicating a reduction in the recirculation zone.

4.4.2. Effect of cylinder size

Fig. 9 shows the streamlines for $D = 0.1$ - $0.4L$. For $Ra = 10^4$ and 10^5 (Fig. 9 (a)–(b)), the streamlines are symmetric about the vertical centreline irrespective of the size variation. When the cylinder size increases, the region between the two cylinders reduces. Hence, more recirculation occurs in this region, which is occupied by the hotter fluid. Figs. 9 (a) and Fig. 10 (a) shows the streamlines and thermal contours obtained for $Ra = 10^4$. Recirculation occurs in the left and right sections of the enclosure about the vertical centreline. For $Da = 10^{-6}$, with a change in diameter from 0.1 to $0.4L$, the distance between the outermost eddy of the left and right section of the enclosure increases. As the Darcy value rises to 10^{-4}, a small amount of fluid passing through the outer boundary of cylinders is seen. At $D = 0.4L$, an increased quantity of fluid entering the cylinder can be observed. At $Da = 10^{-2}$, a substantial amount of fluid enters the cylinders regardless of D. The innermost eddy shifts downwards as the diameter of the cylinder increases from $0.1L$ to $0.4L$. In Fig. 10 (a) (i)-(iii), with rise in Darcy number from 10^{-6} to 10^{-2}, for $D = 0.1L$, the isotherms around the lower cylinder point in the upward direction. A larger cylinder diameter decreases the distance between cylinders. Consequently, the zone of recirculation shrinks. Close to the cylinder, hot fluid occupies the area. The heated fluid recirculates around the cylinders, indicating more prominent conduction effects. The thermal plumes from the bottom cylinder combine with those from the top cylinder. As the diameter grows to 0.4L (Fig. 10 (a) (x)-(xii)), it can be determined that the heat transfer rate enhances as the area of isotherms with a higher value (=0.9) inside the enclosure expands.

Further, the Rayleigh number is raised to 10^5, and Fig. 9 (b) and 10 (b) illustrate the streamlines and thermal contours. The form of streamlines varies as cylinder diameter rises. Fluid does not enter the cylinder when $Da = 10^{-6}$. Due to stronger convective forces, the volume of fluid entering cylinder is greater at $Da = 10^{-4}$ than it is at $Ra = 10^4$. Large amounts of fluid flow through the cylinders when $Da = 10^{-2}$. With the increase in cylinder diameter from 0.1L to 0.4L, the location of the innermost vortex tends to move closer to the bottom wall of the enclosure. Isotherms often gravitate toward top wall.

The thermal plumes from bottom cylinder in Fig. 10 (b) (i)-(vi) tip upwards for $D = 0.1L$ and $0.2L$, and their height rises with Darcy number, signifying a faster rate of heat transfer. The space between the cylinders becomes less as the diameter gets bigger, resulting in recirculation around the bottom cylinder at $0.3L$ and $0.4L$, respectively. The hotter fluid stagnates here. The bottom cylinder's heat transfer rate decreases in contrast to the $0.2L$ case for $Da = 10^{-6}$ and 10^{-4}. On the other hand, when $Da = 10^{-2}$, the rate of heat transfer increases because more fluid is in contact with the heated cylinders and is moving in the direction of the cooled enclosure wall. The area between the cylinders shrinks and is filled with hotter fluids when $D = 0.4L$.

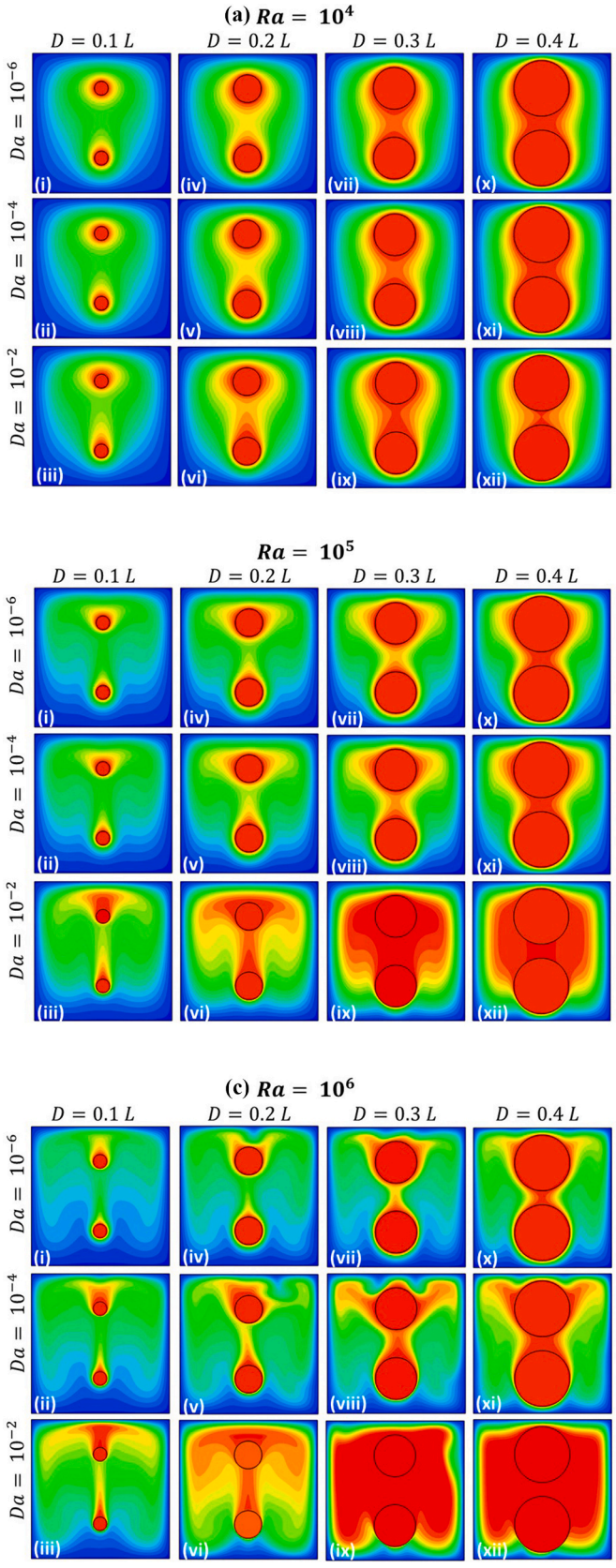

(caption on next page)

Fig. 10. Isotherms around the porous cylinders at (a) $Ra = 10^4$ (b) $Ra = 10^5$ and (c) $Ra = 10^6$ for $Da = 10^{-6}$, 10^{-4} and 10^{-2}.

The flow and thermal fields are affected significantly by increasing Rayleigh number to 10^6. As shown in Figs. 9 (c) and 10 (c), the symmetry of the flow and thermal field distorts. At $Da = 10^{-6}$, in the region with anticlockwise recirculation for $D = 0.2L$, two smaller vortices are observed near the upper cylinder and top wall. Consequently, at $D = 0.3L$, the size of the smaller vortex near the top wall reduces, and it shifts towards the left region of the enclosure. The stronger convective forces allow more fluid to pass through the cylinders, even at Darcy number 10^{-4}, as the inertial forces weaken. Large vortices split into small recirculating zones near the top wall, indicating hotter fluid near the upper cylinder. Upon increasing Darcy number to 10^{-2} (Fig. 9 (c) (vii)-(ix)), large amounts of fluid enter the cylinders. For $D = 0.1L$, small recirculating regions near the bottom wall are observed. As the diameter increases to $0.2L$, additional smaller vortices are noticed inside the larger eddy near the left and right regions of the cylinders, with the most miniature inner eddy near the bottom wall. Smaller eddies merge on further increasing the diameter of cylinders to $D = 0.3L$, and the eye of the most miniature eddy tends to move towards the bottom wall. The eddies near the bottom wall diminish at $D = 0.4L$. Also, an enlarged region with clockwise recirculation pointing towards the top-right corner is seen.

Furthermore, at Rayleigh number 10^6 and $D = 0.1L$, thermal plumes from the lower cylinder point upwards. With increasing the diameter of the cylinder to $0.2L$, when $Da = 10^{-6}$ (Fig. 10 (c) (iv)), the shape of plumes around the upper cylinder changes, and it points towards the top corners of the enclosure, indicating more heat transfer in that direction. With increasing Darcy level to 10^{-4}, a slight change in the inclination of isotherms around the upper cylinder is observed. At $Da = 10^{-2}$, the higher temperature levels above the upper cylinder and in space between the cylinders are observed, indicating an increased heat transfer rate. In the case of $D = 0.4L$ (Fig. 10(c) (x)-(xii)) and Darcy number 10^{-2}, plumes with higher temperature levels spread towards the walls indicating higher amounts of heated fluid moving towards the walls and the corners, enhancing higher heat dissipation.

5. Conclusions

Numerical simulations are carried out using LBM technique to study the influence of *Da, Ra* and cylinder size on natural convection heat transfer from two heated porous cylinders arranged vertically in a cooled enclosure.

- For all the Rayleigh numbers considered, the flow and thermal fields inside the enclosure are found to be steady. These flow and thermal patterns are symmetrical for $Ra = 10^4$ and 10^5 irrespective of variation in Darcy number and diameter of cylinders. With further increasing Rayleigh number to 10^6, asymmetry emerges due to enhanced convective forces.
- As the Darcy number increases, with higher permeability, more fluid comes in contact with the heated cylinders. The density of thermal contours increases near the enclosure walls when $Da = 10^{-2}$. With rise in permeability levels, the heat transfer enhances.
- As the cylinder diameter varies from $0.1L$ to $0.4L$, the distance between the walls and cylinders reduces. In the case of $D = 0.4L$, more fluid recirculates between cylinders and thick isotherms are observed. Also, as the area of fluid flow inside the enclosure shrinks, streamlines and isotherms concentrate more over the surface of cylinders.
- The heat transfer enhancement ratio elevates with Rayleigh and Darcy numbers. At $Ra = 10^4$, the variation is minimal. For $Ra = 10^6$, the enhancement rate is maximum for $D = 0.1L$.
- At $Ra = 10^4$ and $Da = 10^{-6}$, heat transfer enhances by 41.5% when the diameter of the cylinders is doubled. Subsequently, when the diameter is increased four times, the enhancement is 211%.
- In general, it is deduced that with the increment in diameter of the cylinder, the Nu_{Mean} of enclosure rises, but at $Ra = 10^6$, the enhancement rate of Nu_{Mean} value from $D = 0.2L$ to $D = 0.3L$ is less in comparison to the enhancement from $D = 0.1$L – 0.2L.

Author statement

This manuscript is not published and is not under consideration for publication elsewhere. We have no conflicts of interest to disclose.

Declaration of competing interest

The authors declare that they have no known competing financial interests or personal relationships that could have appeared to influence the work reported in this paper.

Data availability

Data will be made available on request.

Acknowledgement

The grant received from the Science and Engineering Research Board (SERB), Government of India, through a project grant (MTR/2019/001440) is acknowledged by one of the authors, S. Dhinakaran.

References

[1] S. Dhinakaran, J. Ponmozhi, Heat transfers from a permeable square cylinder to a flowing fluid, Energy Convers. Manag. 52 (5) (2011) 2170–2182.

[2] B. Shruti, M.M. Alam, A. Parkash, S. Dhinakaran, LBM study of natural convection heat transfer from a porous cylinder in an enclosure, Theor. Comput. Fluid Dynam. 36 (2022) 943–967.
[3] A.I. Alsabery, M.A. Sheremet, A.J. Chamkha, I. Hashim, Conjugate natural convection of Al_2O_3–water nanofluid in a square cavity with a concentric solid insert using Buongiorno's two-phase model, Int. J. Mech. Sci. 136 (2018) 200–219.
[4] F. Moukalled, S. Acharya, Natural convection in the annulus between concentric horizontal circular and square cylinders, J. Thermophys. Heat Tran. 10 (3) (1996) 524–531.
[5] D.G. Roychowdhury, S.K. Das, T. Sundararajan, Numerical simulation of natural convective heat transfer and fluid flow around a heated cylinder inside an enclosure, Heat Mass Tran. 38 (7) (2002) 565–576.
[6] S.A. Nabavizadeh, S. Talebi, M. Sefid, M. Nourmohammadzadeh, Natural convection in a square cavity containing a sinusoidal cylinder, Int. J. Therm. Sci. 51 (2012) 112–120.
[7] M. Jami, A. Mezrhab, M. Bouzidi, P. Lallemand, Lattice Boltzmann method applied to the laminar natural convection in an enclosure with a heat-generating cylinder conducting body, Int. J. Therm. Sci. 46 (1) (2007) 38–47.
[8] M. Jami, A. Mezrhab, H. Naji, Numerical study of natural convection in a square cavity containing a cylinder using the lattice Boltzmann method, Eng. Comput. 25 (5) (2008) 480–489.
[9] B.S. Kim, D.S. Lee, M.Y. Ha, H.S. Yoon, A numerical study of natural convection in a square enclosure with a circular cylinder at different vertical locations, Int. J. Heat Mass Tran. 51 (7–8) (2008) 1888–1906.
[10] S.H. Hussain, A.K. Hussein, Numerical investigation of natural convection phenomena in a uniformly heated circular cylinder immersed in square enclosure filled with air at different vertical locations, Int. Commun. Heat Mass Tran. 37 (8) (2010) 1115–1126.
[11] H.S. Yoon, M.Y. Ha, B.S. Kim, D.H. Yu, Effect of the position of a circular cylinder in a square enclosure on natural convection at Rayleigh number of 10^7, Phys. Fluids 21 (4) (2009), 047101.
[12] D.H. Kang, M.Y. Ha, H.S. Yoon, C. Choi, Bifurcation to unsteady natural convection in square enclosure with a circular cylinder at Rayleigh number of 10^7, Int. J. Heat Mass Tran. 64 (2013) 926–944.
[13] P. Nithiarasu, K.N. Seetharamu, T. Sundararajan, Natural convective heat transfer in a fluid saturated variable porosity medium, Int. J. Heat Mass Tran. 40 (16) (1997) 3955–3967.
[14] T.R. Vijaybabu, Influence of permeable circular body and $CuO-H_2O$ nanofluid on buoyancy-driven flow and entropy generation, Int. J. Mech. Sci. 166 (2020), 105240.
[15] J.T. Hu, S.J. Mei, Combined thermal and moisture convection and entropy generation in an inclined rectangular enclosure partially saturated with porous wall: nonlinear effects with Soret and Dufour numbers, Int. J. Mech. Sci. 199 (2021), 106412.
[16] H.S. Yoon, J. H Jung, Y.G. Park, Natural convection in a square enclosure with two horizontal cylinders, Numer. Heat Tran., Part A: Applications 62 (9) (2012) 701–721.
[17] H. Yüncü, A. Batta, Effect of vertical separation distance on laminar natural convective heat transfer over two vertically spaced equitemperature horizontal cylinders, Appl. Sci. Res. 52 (3) (1994) 259–277.
[18] H.S. Yoon, Y.G. Park, J.H. Jung, Natural convection in a square enclosure with differentially heated two horizontal cylinders, Numer. Heat Tran., Part A: Applications 65 (4) (2014) 302–326.
[19] E.M. Sparrow, J.E. Niethammer, Effect of vertical separation distance and cylinder-to-cylinder temperature imbalance on natural convection for a pair of horizontal cylinders, J. Heat Tran. 103 (4) (1981) 638–644.
[20] M. Corcione, Correlating equations for free convection heat transfer from horizontal isothermal cylinders set in a vertical array, Int. J. Heat Mass Tran. 48 (17) (2005) 3660–3673.
[21] M.S. Chae, B.J. Chung, Effect of pitch-to-diameter ratio on the natural convection heat transfer of two vertically aligned horizontal cylinders, Chem. Eng. Sci. 66 (21) (2011) 5321–5329.
[22] O. Reymond, D.B. Murray, T.S. O'Donovan, Natural convection heat transfer from two horizontal cylinders, Exp. Therm. Fluid Sci. 32 (8) (2008) 1702–1709.
[23] M. Lacroix, Natural convection heat transfer around two heated horizontal cylinders inside a rectangular cavity cooled from above, Numer. Heat Tran. 21 (1) (1992) 37–54.
[24] M. Lacroix, A. Joyeux, Coupling of wall conduction with natural convection from heated cylinders in a rectangular enclosure, Int. Commun. Heat Mass Tran. 23 (1) (1996) 143–151.
[25] Y.G. Park, M.Y. Ha, C. Choi, J. Park, Natural convection in a square enclosure with two inner circular cylinders positioned at different vertical locations, Int. J. Heat Mass Tran. 77 (2014) 501–518.
[26] Y.G. Park, M.Y. Ha, H.S. Yoon, Study on natural convection in a cold square enclosure with a pair of hot horizontal cylinders positioned at different vertical locations, Int. J. Heat Mass Tran. 65 (2013) 696–712.
[27] H.W. Cho, Y.M. Seo, G.S. Mun, M.Y. Ha, Y.G. Park, The effect of instability flow for two-dimensional natural convection in a square enclosure with different arrays of two inner cylinders, Int. J. Heat Mass Tran. 114 (2017) 307–317.
[28] N. Goswami, P.R. Randive, S. Pati, Natural convection from a pair of heated cylinders in a square cavity with non-uniform temperature on the side walls, *J. Inst. Eng.*: Series C 102 (2) (2021) 389–396.
[29] G.C. Pal, G. Nammi, S. Pati, P.R. Randive, Natural convection in an enclosure with a pair of cylinders under magnetic field, Case Stud. Therm. Eng. (2022), 101763.
[30] Y.M. Seo, et al., Two-dimensional flow instability induced by natural convection in a square enclosure with four inner cylinders. Part II: effect of various positions of inner cylinders, Int. J. Heat Mass Tran. 113 (2017) 1319–1331.
[31] S.A. M Mehryan, M. Ghalambaz, A.J. Chamkha, M. Izadi, Numerical study on natural convection of Ag–MgO hybrid/water nanofluid inside a porous enclosure: a local thermal non-equilibrium model, Powder Technol. 367 (2020) 443–455.
[32] M. Ghalambaz, S.A. M Mehryan, A. Hajjar, A. Veismoradi, Unsteady natural convection flow of a suspension comprising Nano-Encapsulated Phase Change Materials (NEPCMs) in a porous medium, Adv. Powder Technol. 31 (3) (2020) 954–966.
[33] M. Ghalambaz, T. Groşan, I. Pop, Mixed convection boundary layer flow and heat transfer over a vertical plate embedded in a porous medium filled with a suspension of nano-encapsulated phase change materials, J. Mol. Liq. 293 (2019), 111432.
[34] M. Ghalambaz, S.A. M Mehryan, I. Zahmatkesh, A. Chamkha, Free convection heat transfer analysis of a suspension of nano–encapsulated phase change materials (NEPCMs) in an inclined porous cavity, Int. J. Therm. Sci. 157 (2020), 106503.
[35] K. Hosseinzadeh, M.A.E. Moghaddam, S.K. Nateghi, M.B. Shafii, D.D. Ganji, Radiation and convection heat transfer optimization with MHD analysis of a hybrid nanofluid within a wavy porous enclosure, J. Magn. Magn Mater. 566 (2023), 170328.
[36] F. Selimefendigil, H.F. Öztop, Combined effects of using multiple porous cylinders and inclined magnetic field on the performance of hybrid nanoliquid forced convection, J. Magn. Magn Mater. 565 (2023), 170137.
[37] A. Fedotov, Y. Tsitavets, A. Elyshev, Numerical study of free convection in a thin layer between coaxial horizontal cylinders, Case Stud. Therm. Eng. 41 (2023), 102606.
[38] J. Chordiya, R.V. Sharma, Numerical analysis of the longitudinal size of the partition on natural convection heat transfer and fluid flow within a differentially heated porous enclosure, Heat Transfer 52 (2023) 890–910.
[39] T. Tayebi, F. Dahmane, W. Jamshed, A.J. Chamkha, S.M. El Din, Z. Raizah, Double-diffusive magneto-natural convection of nanofluid in an enclosure equipped with a wavy porous cylinder in the local thermal non-equilibrium situation, Case Stud. Therm. Eng. 43 (2023), 102785.
[40] S. Javed, S. Saha, Estimation of comprehensive thermal performance for conjugate natural convection inside a dome-shaped porous chamber holding a solid cylinder, Results in Engineering (2023), 100896.
[41] N.K. Reddy, H.K. Swamy, M. Sankar, B. Jang, MHD convective flow of Ag-TiO2 hybrid nanofluid in an inclined porous annulus with internal heat generation, Case Stud. Therm. Eng. (2023), 102719.

[42] A. Abderrahmane, A. Manoongam, A.A. Alizadeh, O. Younis, H. Zekri, S.S.P. M Isa, K. Guedri, Investigation of the free convection of nanofluid flow in a wavy porous enclosure subjected to a magnetic field using the Galerkin finite element method, J. Magn. Magn Mater. 569 (2023), 170446.
[43] Z. Guo, T.S. Zhao, Lattice Boltzmann model for incompressible flows through porous media, Phys. Rev. 66 (3) (2002), 036304.
[44] G. Lauriat, V. Prasad, Non-Darcian effects on natural convection in a vertical porous enclosure, Int. J. Heat Mass Tran. 32 (1989) 2135–2148.
[45] A.A. Mohamad, Lattice Boltzmann Method: Fundamentals and Engineering Applications with Computer Codes, Springer Science & Business Media, London, 2011.
[46] M.C. Sukop, D.T. Thorne, Lattice Boltzmann Modeling: an Introduction for Geoscientists and Engineers, second ed., Springer Berlin Heidelberg, New York, 2006, 978-3-642-06625-2.
[47] J. Kozeny, Ueber kapillare Leitung des Wassers im Boden. Sitzungsber Akad. Wiss., Wien, Royal Academy of Science, Vienna, Proc. Class I, 1927, pp. 271–306, 136(2a.
[48] P.C. Carman, Fluid flow through granular beds, Trans. Inst. Chem. Eng. 15 (1937) 150–166.
[49] P.C. Carman, Flow of Gases through Porous Media, Butterworths Scientific Publications, New York, 1956.
[50] P. Yu, Y. Zeng, T.S. Lee, X.B. Chen, H.T. Low, Steady flow around and through a permeable circular cylinder, Comput. Fluid 42 (1) (2011) 1–12.